Supporting Information for the manuscript:

A self-assembling of a metal-organic cage-like structure bearing cofacial redox-active bis-(o-semiquinone) copper(II) units

Anna V. Cherkasova, Anton V. Cherkasov, Konstantin A. Martyanov, Artem S. Bogomyakov, V. N. Khrustalev, Alexander A. Kissel, Konstantin A. Kozhanov, Viacheslav A. Kuropatov* and Vladimir K. Cherkasov

Table of Contents

Compounds formulae

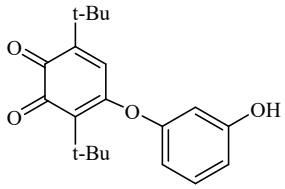

quinone **1a**

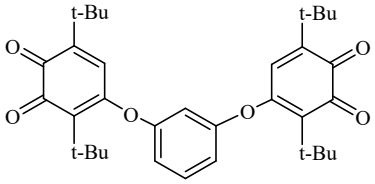

quinone **1**

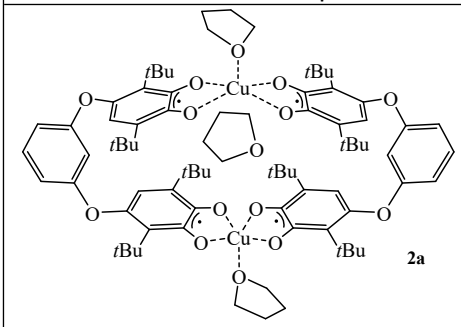

Complex **2a**

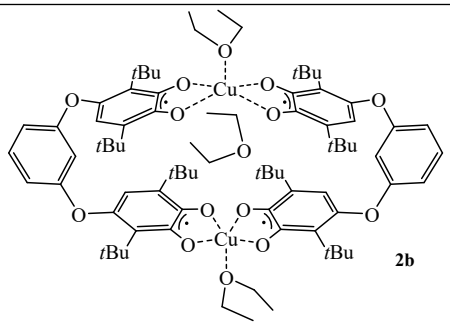

Complex **2b**

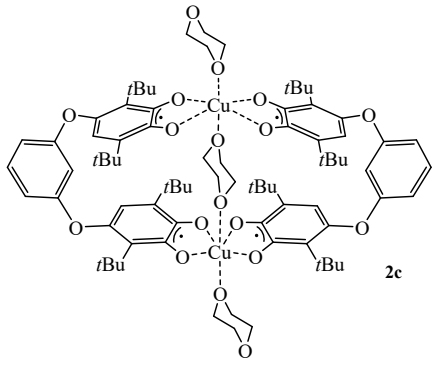

Complex **2c**

X-ray diffractometry data

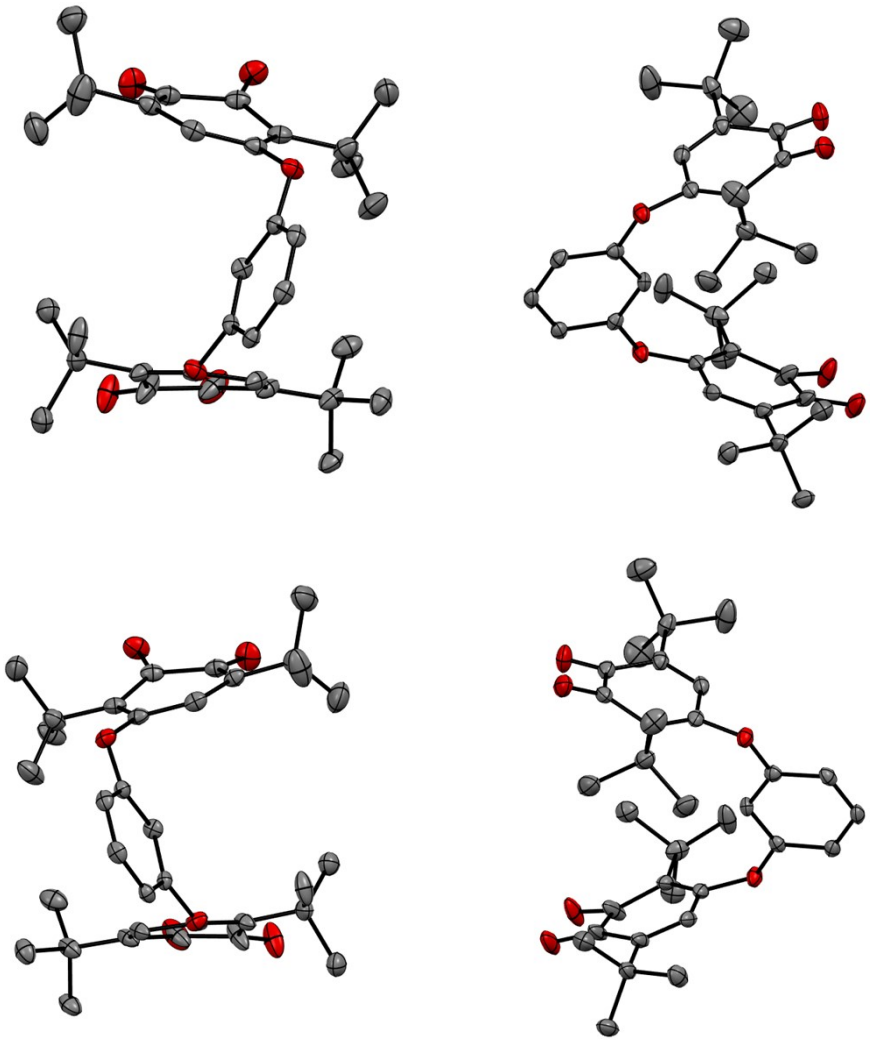

Figure SI1. Enantiomeric forms of the ligand (top and bottom)

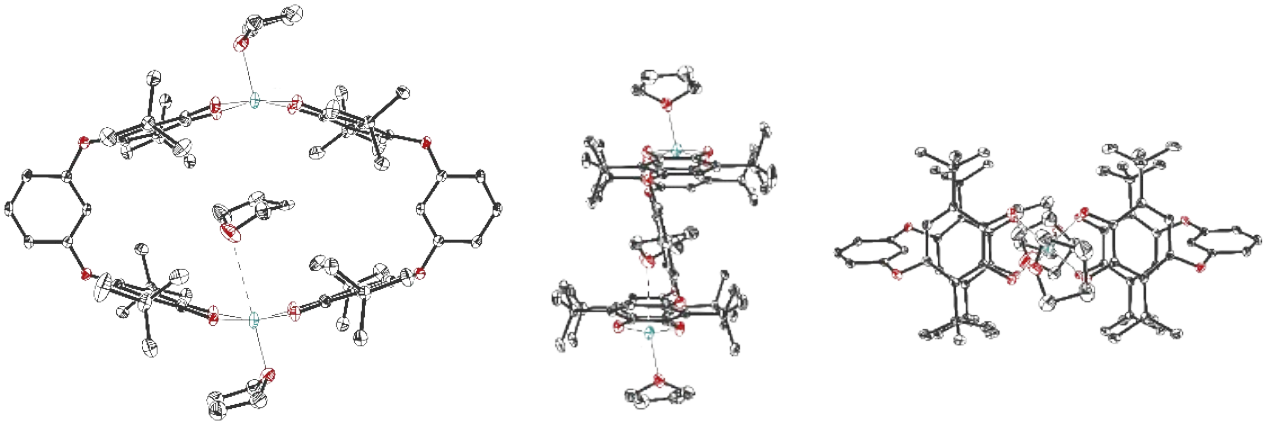

Figure SI2. Front (*a*), side (*b*) and above (*c*) view of cage **2a**. Thermal ellipsoids are given with 30% probability level. All hydrogen atoms are omitted for clarity. Color code: Cu, blue; O, red; C, black.

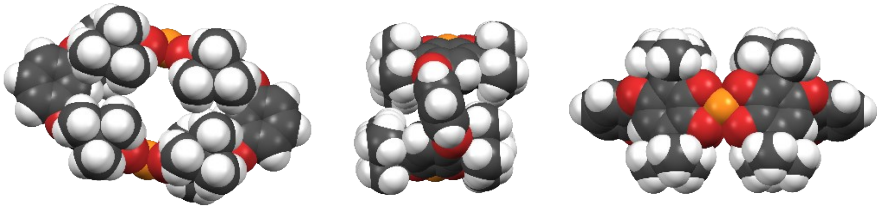

Fig. SI3. Front (*a*), side (*b*) and above (*c*) view of cage **2a** in space-filling representation. Color code: Cu, orange; O, red; C, grey; H, white.

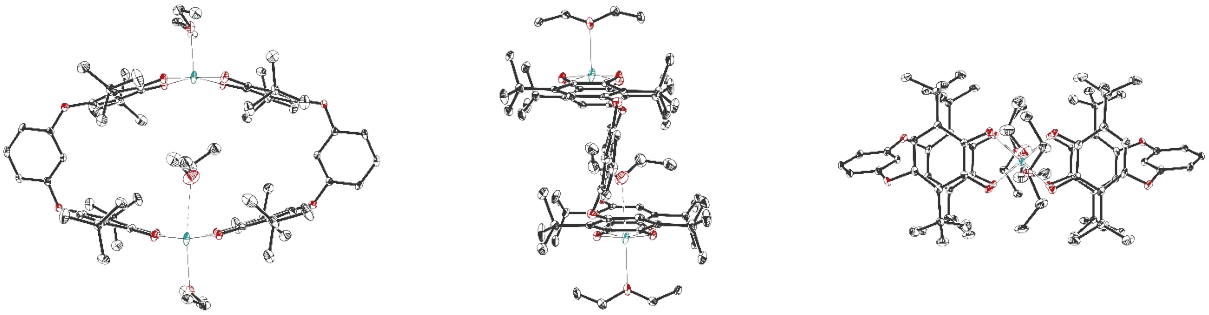

Figure SI4. Front (a), side (b) and above (c) view of cage **2b**. Thermal ellipsoids are given with 30% probability level. All hydrogen atoms are omitted for clarity. Color code: Cu, blue; O, red; C, black.

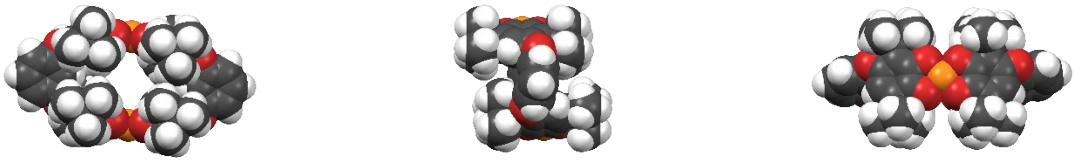

Fig. SI5. Front (*a*), side (*b*) and above (*c*) view of cage **2b** in space-filling representation. Color code: Cu, orange; O, red; C, grey; H, white.

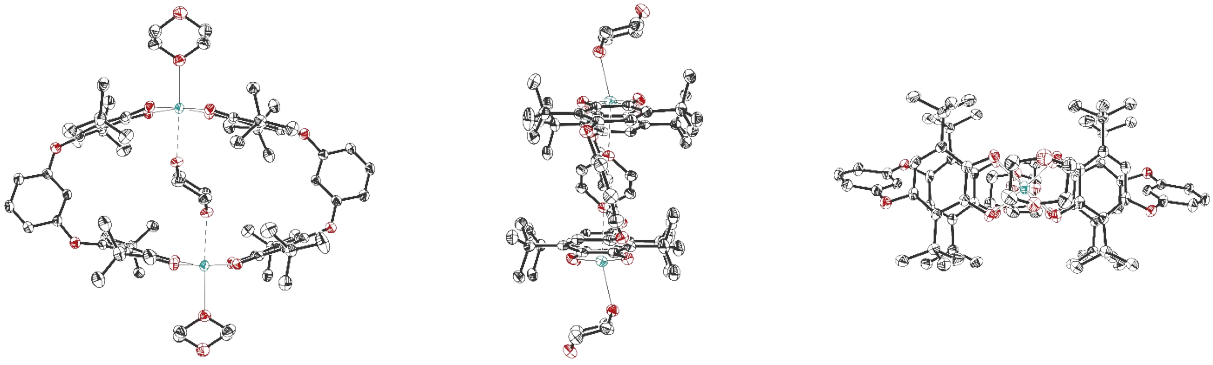

a ***b*** ***c***

Figure SI6. Front (a), side (b) and above (c) view of cage **2c**. Thermal ellipsoids are given with 30% probability level. All hydrogen atoms are omitted for clarity. Color code: Cu, blue; O, red; C, black.

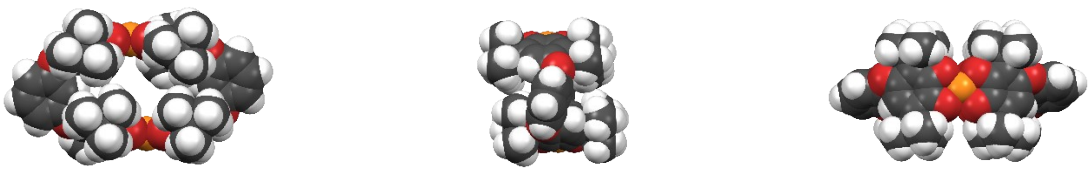

Fig. SI7. Front (*a*), side (*b*) and above (*c*) view of cage **2c** in space-filling representation. Color code: Cu, orange; O, red; C, grey; H, white.

Table SI1. Crystal data and structures refinement details for **1**, **2a-c**.

	1	**2a**	**2b**	**2c**
Formula	$C_{38}H_{48}N_2O_6$	$C_{83.6}H_{122.4}Cu_2O_{18.6}$	$C_{80}H_{114}Cu_2O_{15}$	$C_{86}H_{120}Cu_2O_{21}$
M	628.78	1552.09	1442.79	1616.88
T, K	100.0(2)	100.0(2)	100.0(2)	100.0(2)
λ, Å	0.71073	0.71073	0.71073	0.79313
Crystal system	Triclinic	Triclinic	Triclinic	Monoclinic
Space group	*P-1*	*P-1*	*P-1*	$P2_1/c$
a, Å	9.1464(4)	13.7617(10)	11.2133(5)	14.2710(9)
b, Å	9.8897(4)	13.8309(10)	14.5574(7)	17.2741(14)
c, Å	20.7789(8)	14.3002(10)	14.7287(7)	17.9562(16)
α, deg	77.342(2)	62.027(2)	112.212(2)	90
β, deg	77.4140(10)	63.270(2)	100.457(2)	99.095(10)
γ, deg	76.279(2)	89.914(2)	110.623(2)	90
V, Å^3	1754.03(13)	2069.9(3)	1941.00(16)	4370.9(6)
Z	2	1	1	2
d_{calc}, g/cm$_3$	1.191	1.245	1.234	1.128
μ, mm^{-1}	0.080	0.580	0.610	0.731
F_{000}	676	831	772	1580
Crystal dimensions, mm	0.41×0.27×0.07	0.35×0.29×0.14	0.27×0.23×0.10	0.10×0.07×0.02
ϑ range for data	2.21–27.15	2.74–27.34	2.08–25.06	2.56–30.98
Completeness, %	99.2	99.4	99.6	97.5
HKL indices	$-11 \le h \le 11$	$-17 \le h \le 17$	$-13 \le h \le 13$	$-18 \le h \le 18$
	$-12 \le k \le 12$	$-17 \le k \le 17$	$-17 \le k \le 17$	$-21 \le k \le 21$
	$-26 \le l \le 26$	$-18 \le l \le 18$	$-17 \le l \le 17$	$-23 \le l \le 23$
Reflns. collected	22426	73932	22303	34459
Reflns. unique ($I > 2\sigma(I)$)	5296	6932	4408	7053
R_{int}	0.0405	0.0581	0.0607	0.0426
Data / restraints / parameters	7725 / 81 / 497	9290 / 652 / 619	6868 / 438 / 464	9770 / 18 / 449
$S(F^2)$	1.080	1.061	1.003	1.015
R_1 / wR_2 ($I > 2\sigma(I)$)	0.0554 / 0.1170	0.0712 / 0.1529	0.0675 / 0.1494	0.0801 / 0.1948
R_1 / wR_2 (all data)	0.0929 / 0.1327	0.1019 / 0.1690	0.1230 / 0.1725	0.1057 / 0.2123
Largest diff. peak and hole, e/Å^3	0.33 / -0.43	1.62 / -1.36	0.73 / -0.74	1.08 / -0.78

Table SI2. Selected bond lengths in **1**, **2a**-**c**.

	1	**2a**	**2b**	**2c**
O(1)-C(1)	1.215(2)	1.286(4)	1.285(5)	1.300(5)
O(2)-C(2)	1.208(2)	1.290(4)	1.284(5)	1.293(4)
O(5)-C(21)	1.217(3)	1.286(4)	1.289(5)	1.296(5)
O(6)-C(22)	1.214(2)	1.286(4)	1.290(5)	1.282(5)
C(1)-C(2)	1.557(3)	1.472(5)	1.461(6)	1.460(5)
C(21)-C(22)	1.544(4)	1.469(5)	1.463(6)	1.464(6)
Cu(1)-O(1)		1.942(2)	1.938(3)	1.930(3)
Cu(1)-O(2)		1.924(2)	1.946(3)	1.954(3)
Cu(1)-O(5A)		1.940(3)	1.936(3)	1.931(3)
Cu(1)-O(6A)		1.937(2)	1.940(3)	1.946(3)
Cu(1)-O_{solv}		2.12(2)	2.429(4)	2.399(3)
Cu(1)-O_{guest}		3.21(2)	2.84(2)	2.572(3)

***UV/vis* Measurements**

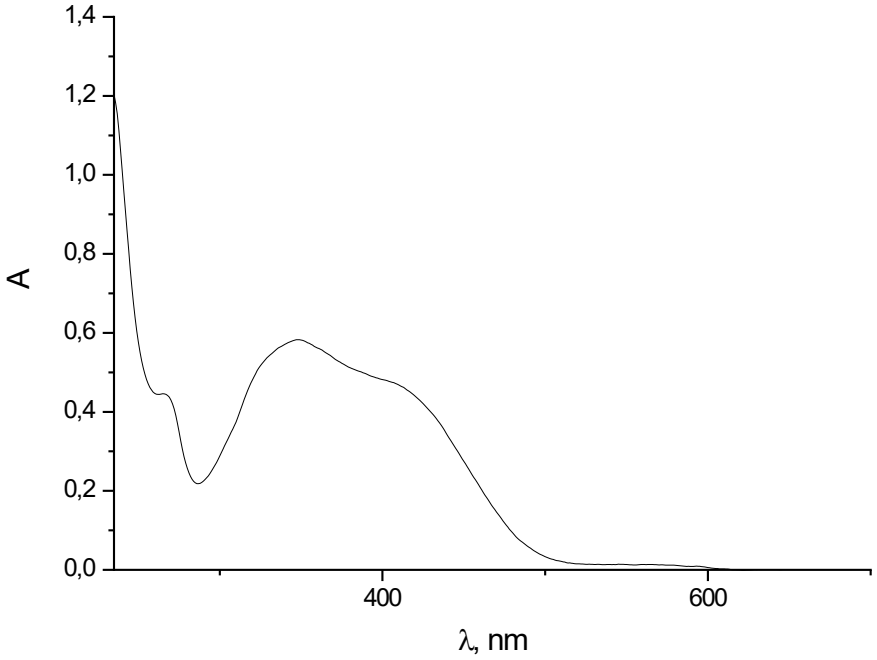

Figure SI8. UV/Vis spectra of species **1** ($1.0*10^{-4}$ M in CH_2Cl_2, *l* = 1 cm), λ_{max}, nm (ε): 269 (4370), 346 (5810), 404 (4770), 564 (140)

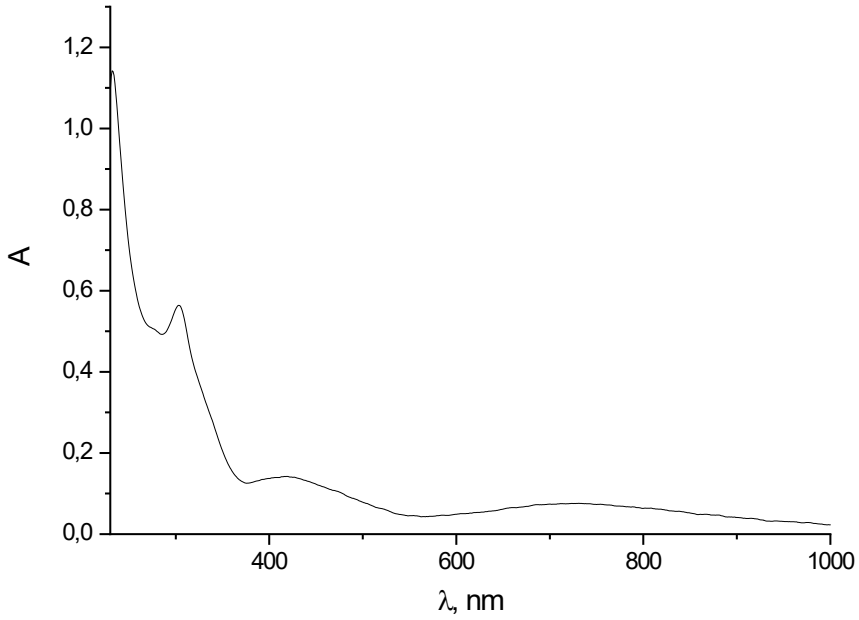

Figure SI9. UV/Vis spectra of species **2a** ($2.5\cdot10^{-5}$ M in CH_2Cl_2, *l* = 1 cm), λ_{max}, nm (ε): 304 (22520), 419 (5680), 728 (3040)

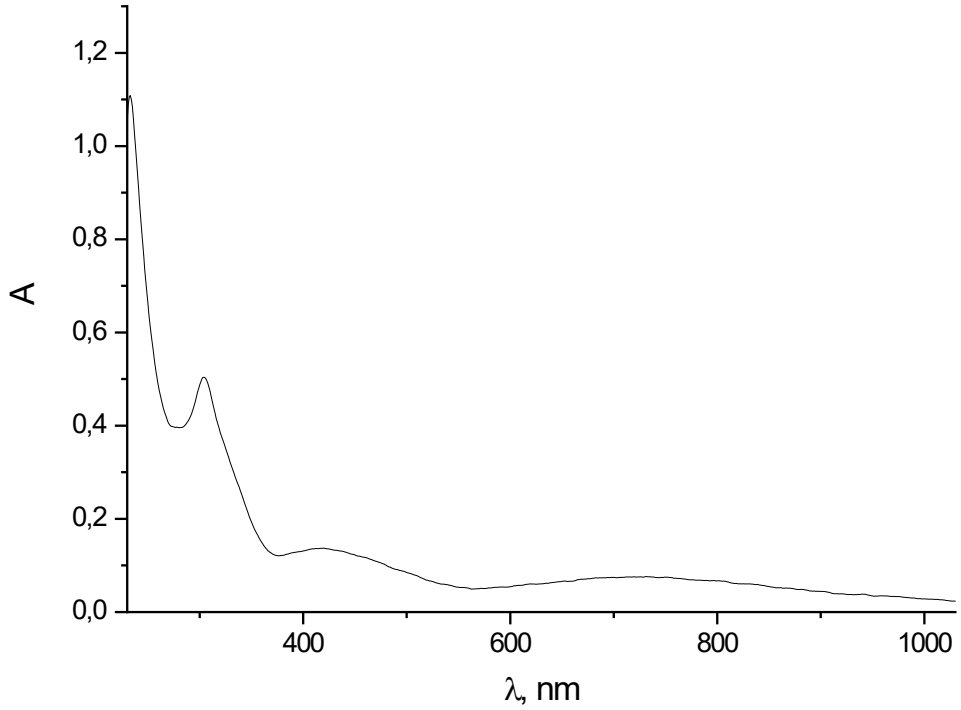

Figure SI10. UV/Vis spectra of species **2b** ($2.5 \cdot 10^{-5}$ M in CH_2Cl_2, l = 1 cm), λ_{max}, nm (ε): 305 (20120), 419 (5480), 725 (3000)

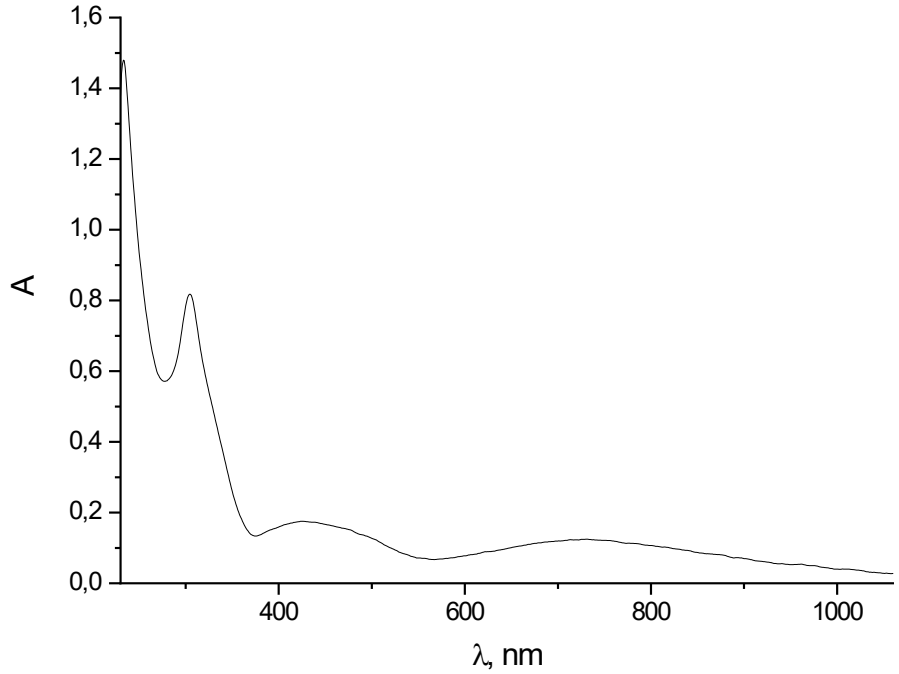

Figure SI11. UV/Vis spectra of species **2c** ($2.5 \cdot 10^{-5}$ M in CH_2Cl_2, l = 1 cm), λ_{max}, nm (ε): 304 (32680), 427 (7000), 729 (4960)

Cyclic voltammetry

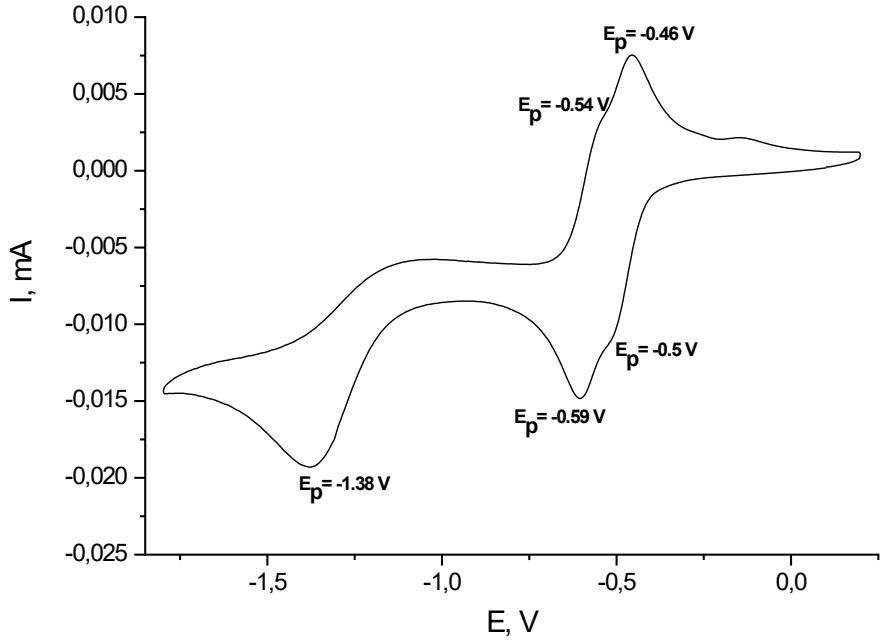

Figure SI12. Cyclic voltammogram of di-o-quinone **1** ($1.0*10^{-3}$ M in CH_2Cl_2, 200 mV/s, 0.2 M Bu_4NClO_4)

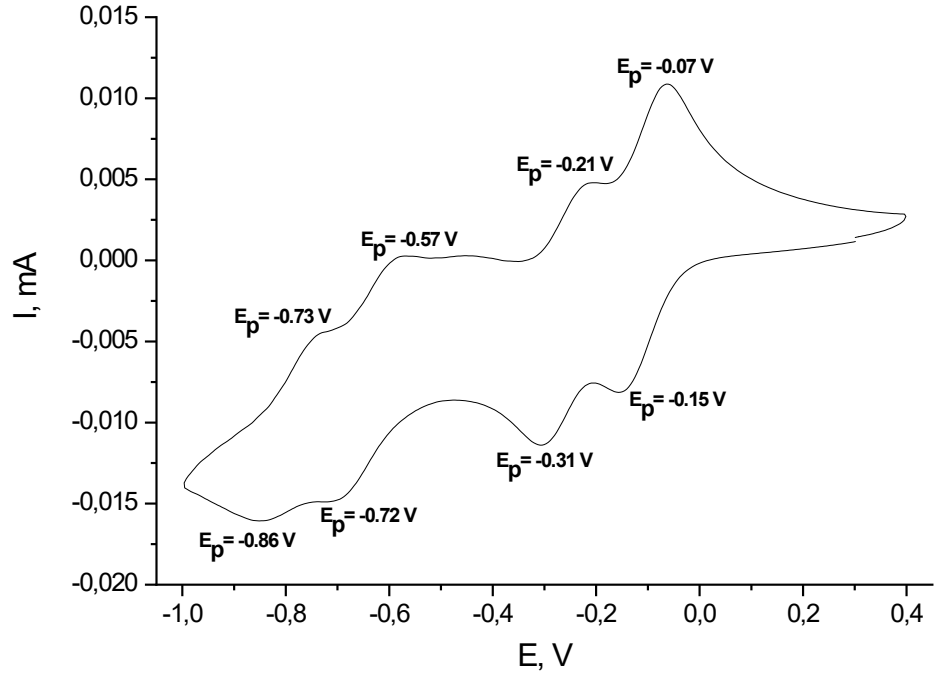

Figure SI13. Cyclic voltammogram of complex **2a** ($1.0*10^{-3}$ M in CH_2Cl_2, 200 mV/s, 0.2 M Bu_4NClO_4)

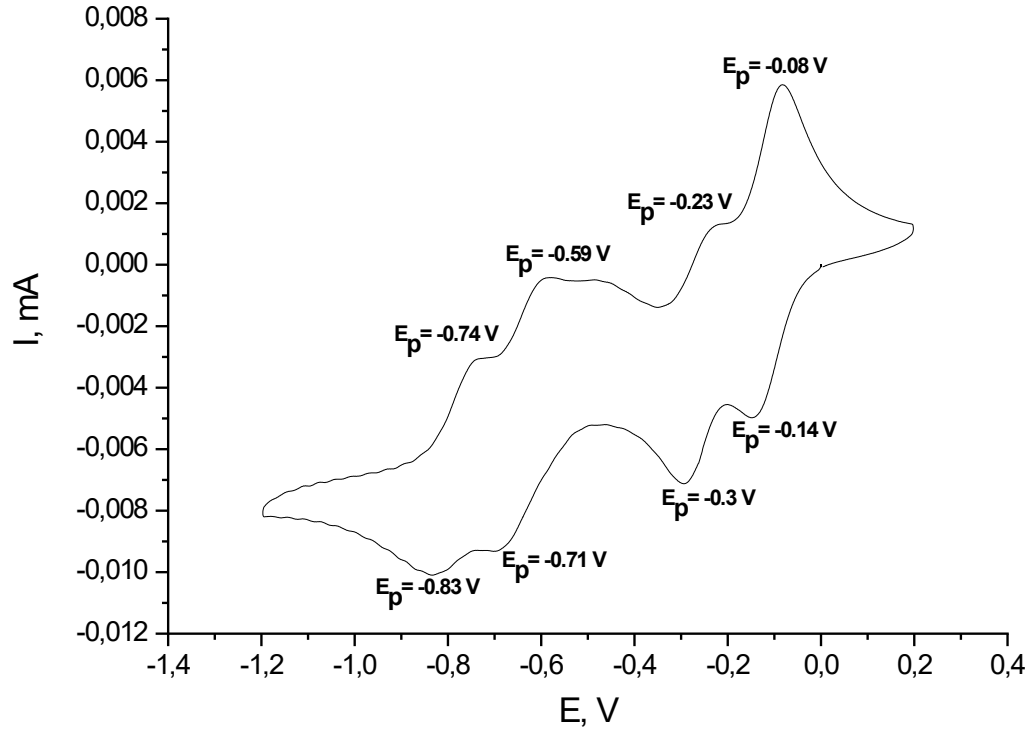

Figure SI14. Cyclic voltammogram of complex **2b** ($1.0*10^{-3}$ M in CH_2Cl_2, 200 mV/s, 0.2 M Bu_4NClO_4)

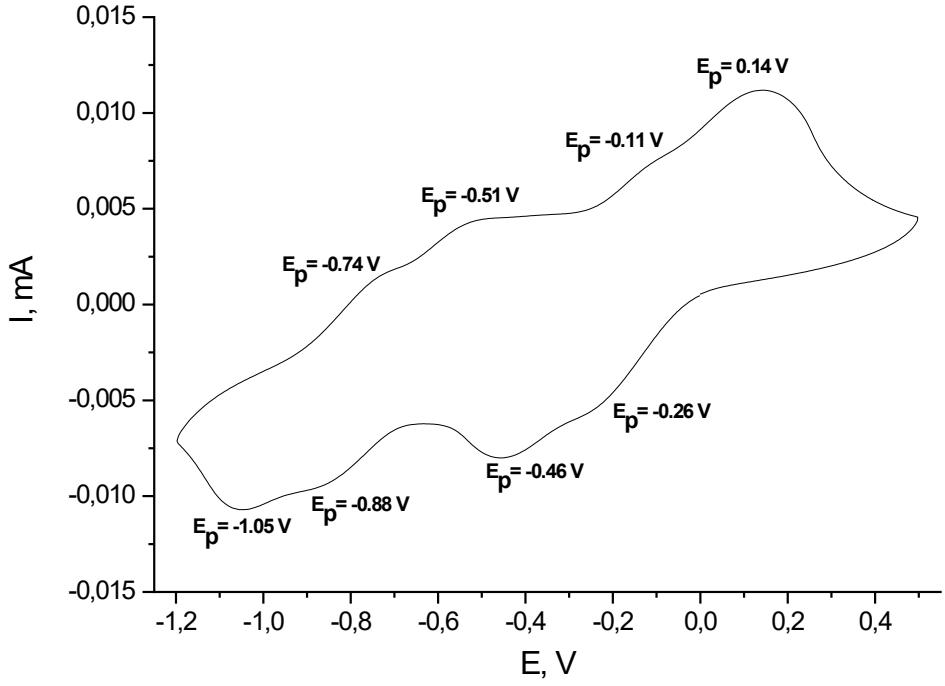

Figure SI15. Cyclic voltammogram of complex **2c** ($1.0*10^{-3}$ M in CH_2Cl_2, 200 mV/s, 0.2 M Bu_4NClO_4)

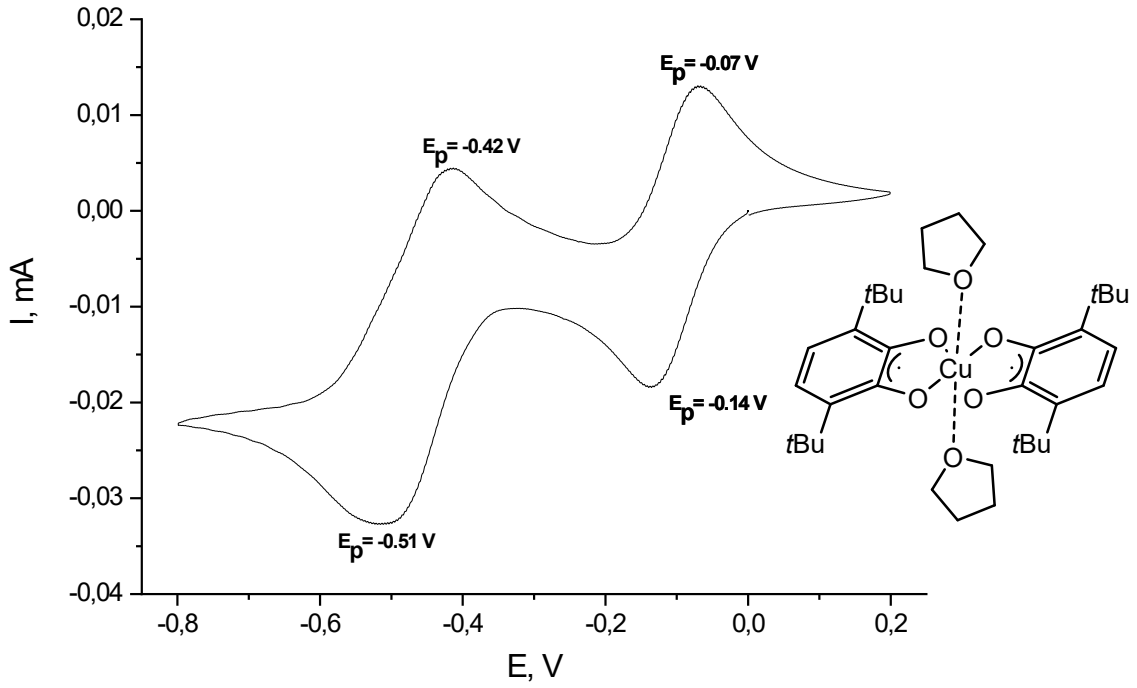

Figure SI16. Cyclic voltammogram of copper bis-3,6-di-tert-butylsemiquinonate (36SQCu) ($1*10^{-3}$ M in CH_2Cl_2, 200 mV/s, 0.2 M Bu_4NClO_4)

IR spectroscopy data

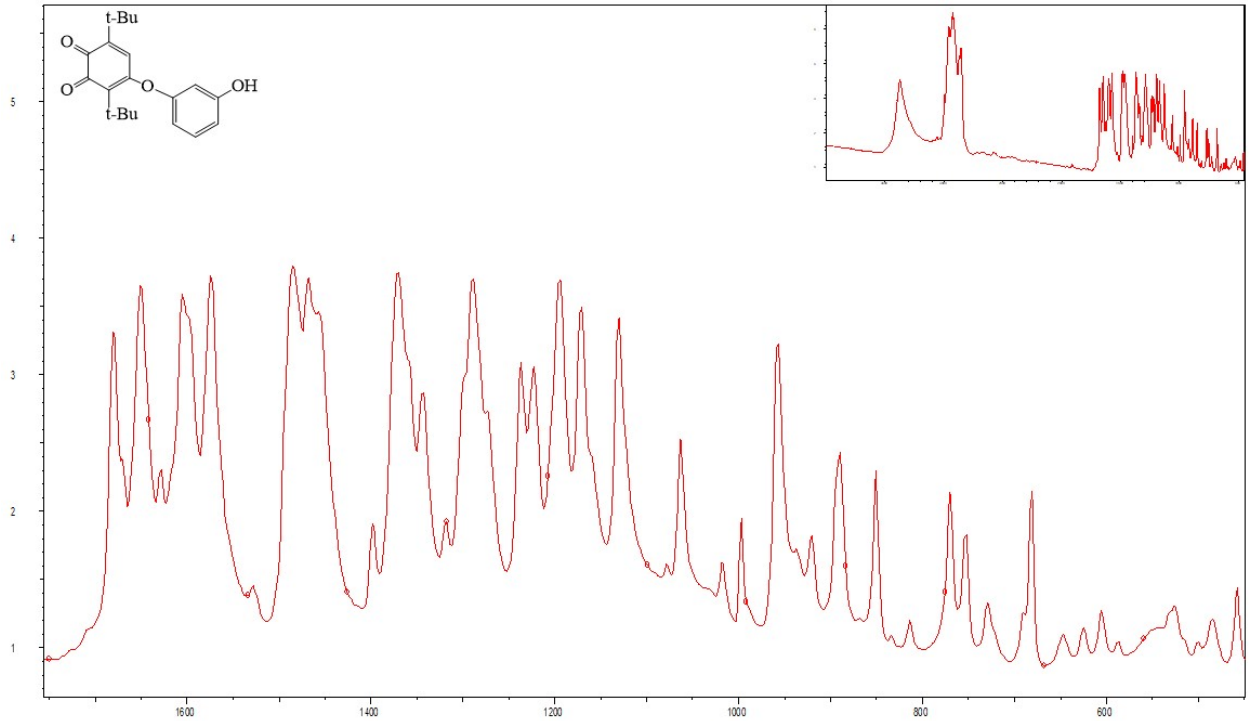

Figure. SI17. IR spectrum of **1a** in nujol.

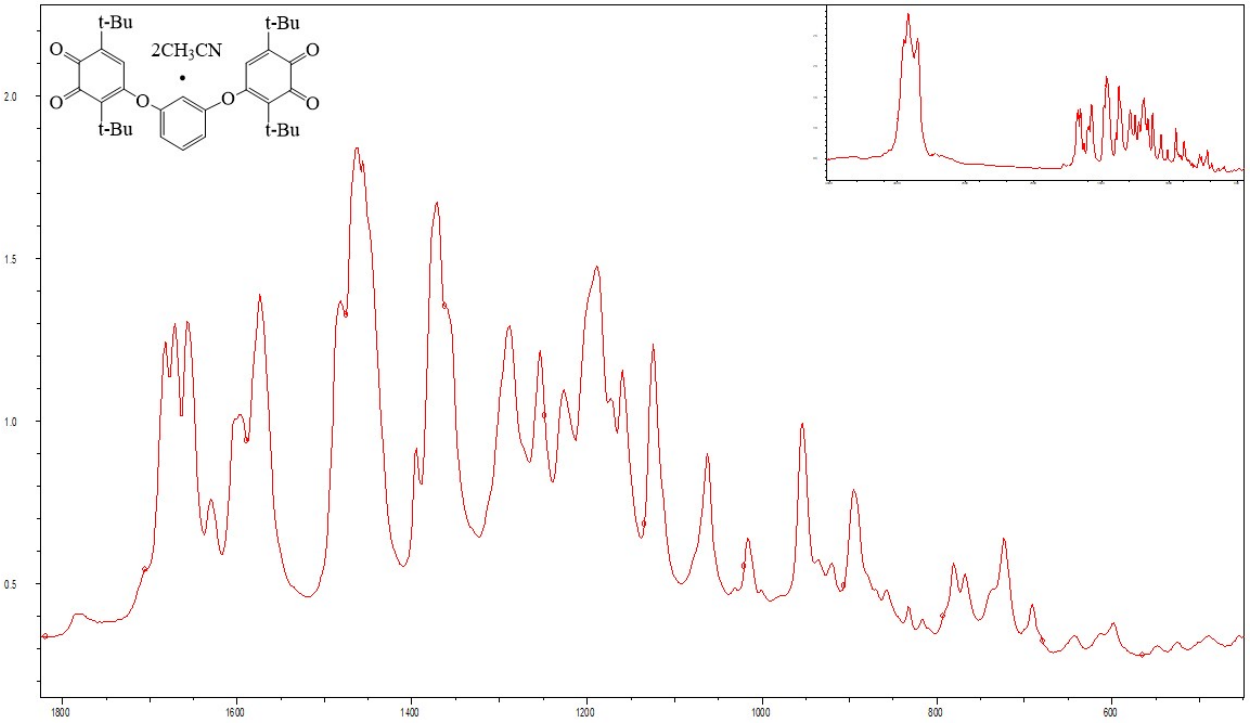

Figure. SI18. IR spectrum of **1** in nujol.

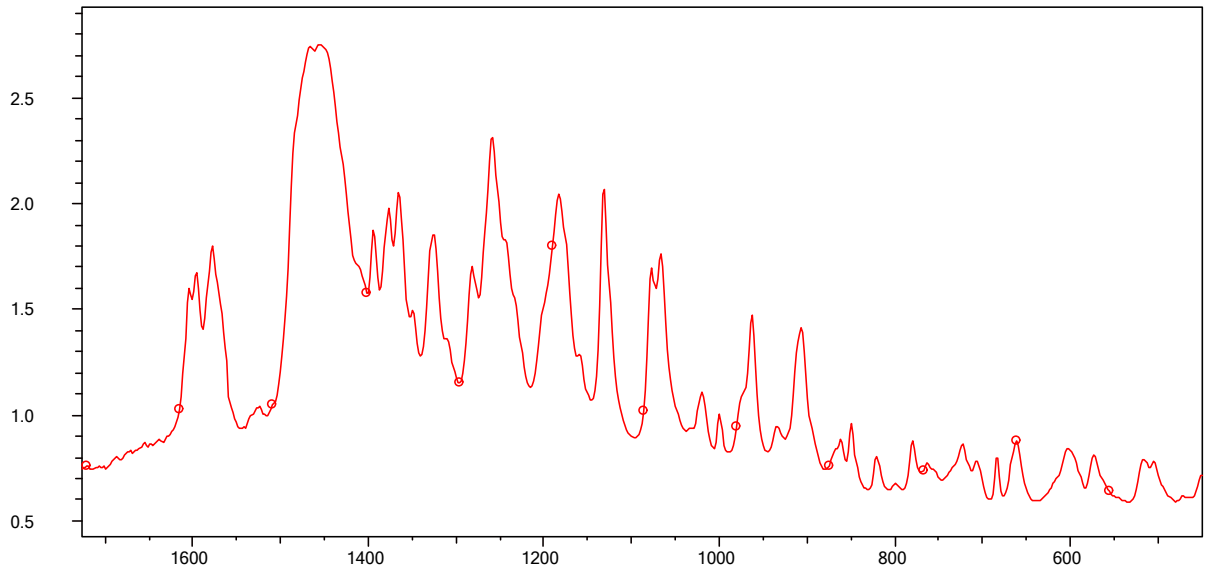

Figure. SI19. IR spectrum of **2a** in nujol.

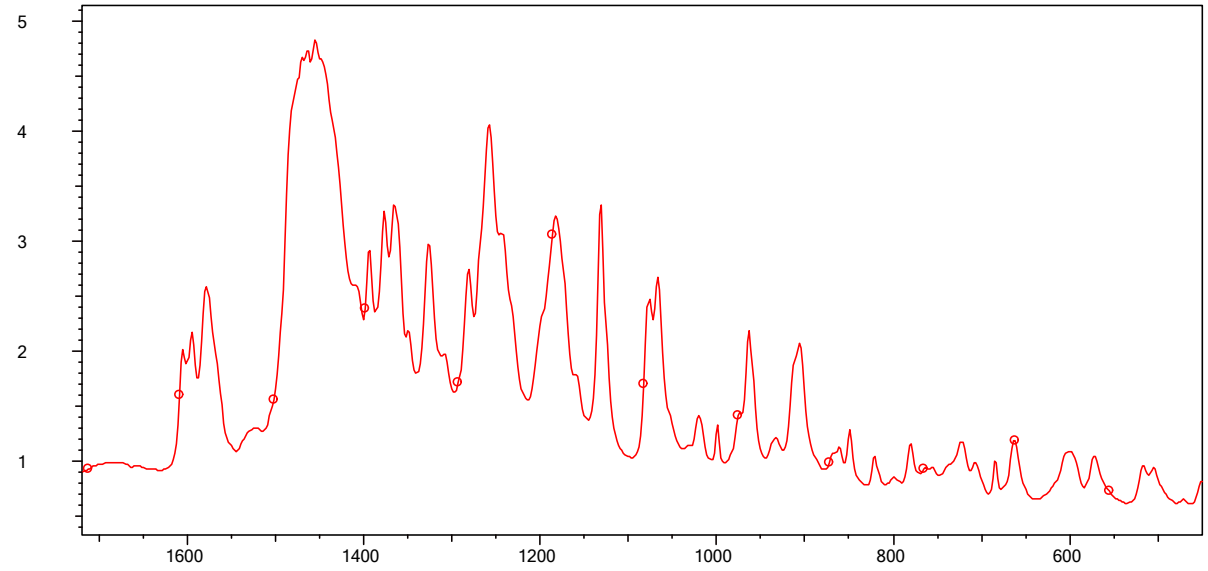

Figure. SI20. IR spectrum of **2b** in nujol.

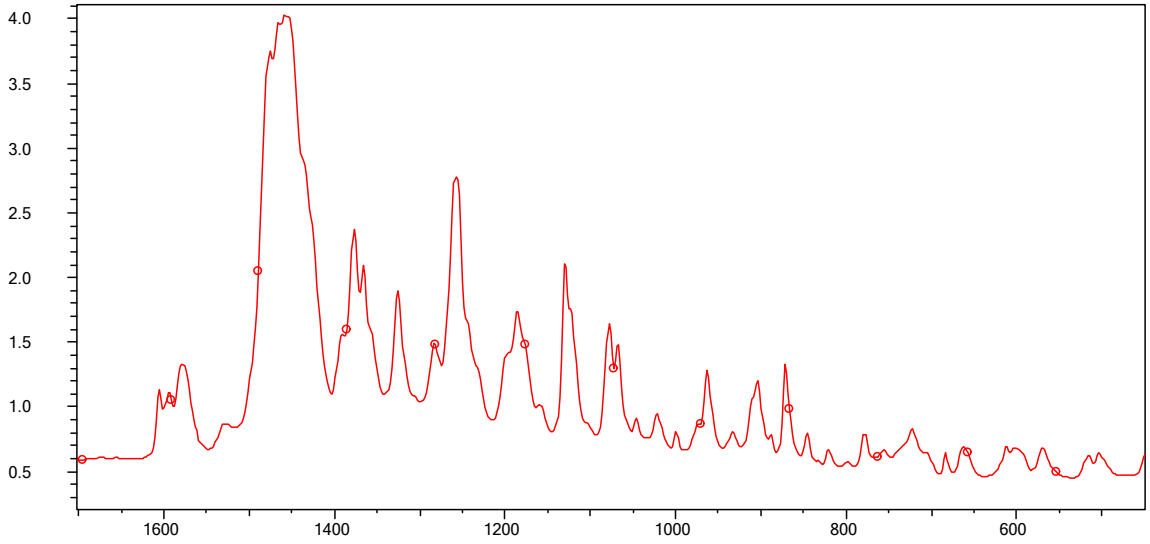

Figure. SI21. IR spectrum of **2c** in nujol.

NMR spectroscopy data

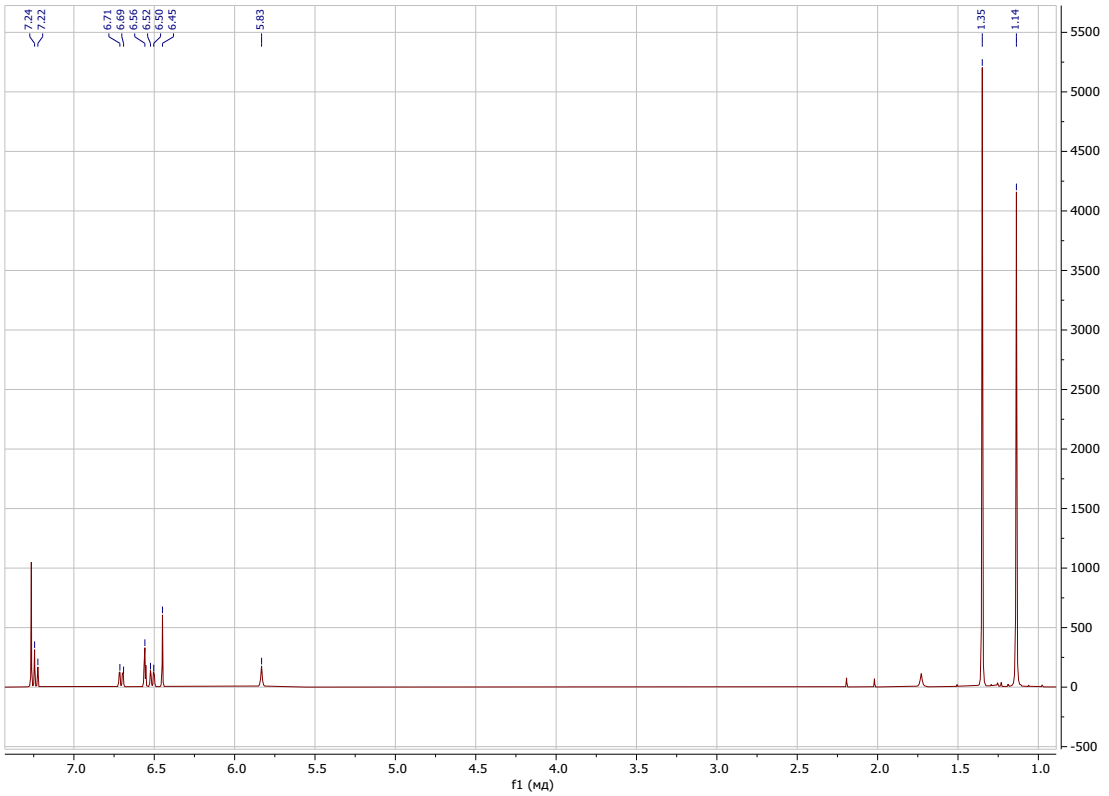

Figure. SI22. ^{1}H NMR spectrum of **1a** ($CDCl_3$)

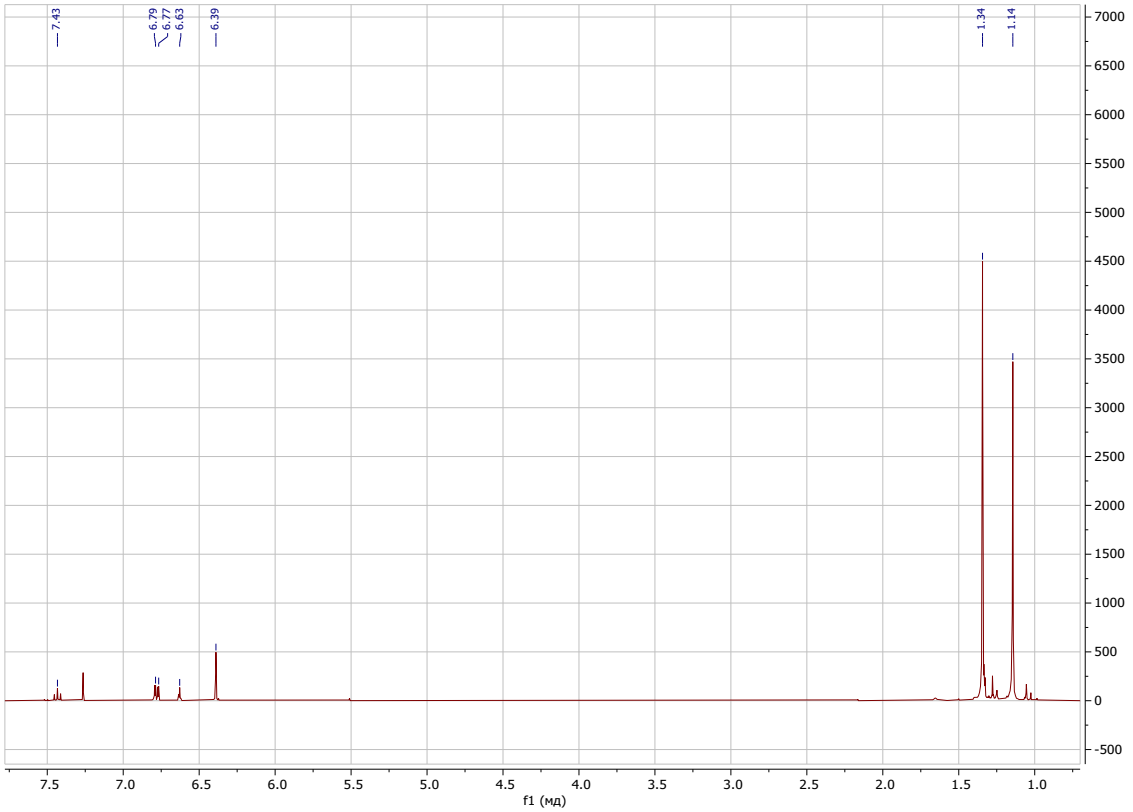

Figure. SI23. ^{1}H NMR spectrum of **1** ($CDCl_3$)

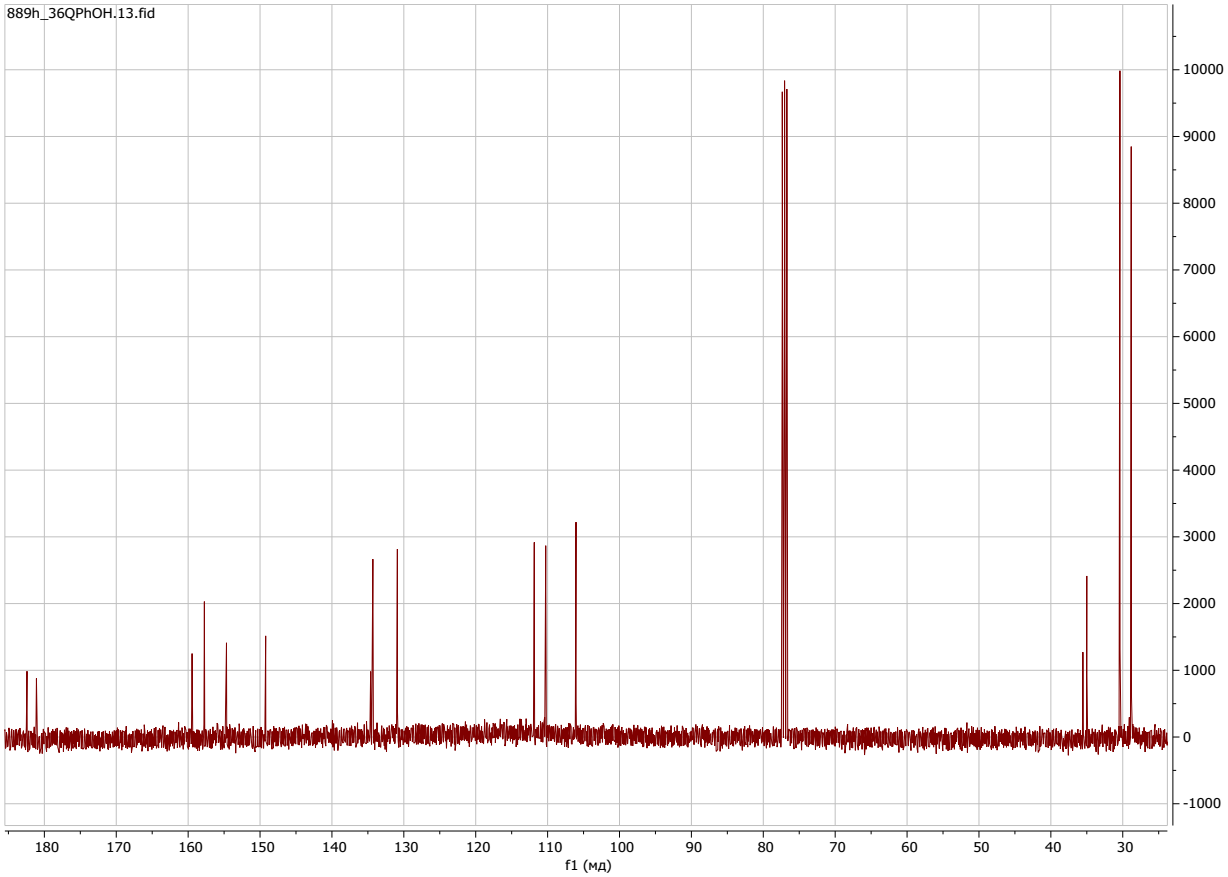

Figure. SI24. ^{13}C NMR spectrum of **1a** ($CDCl_3$)

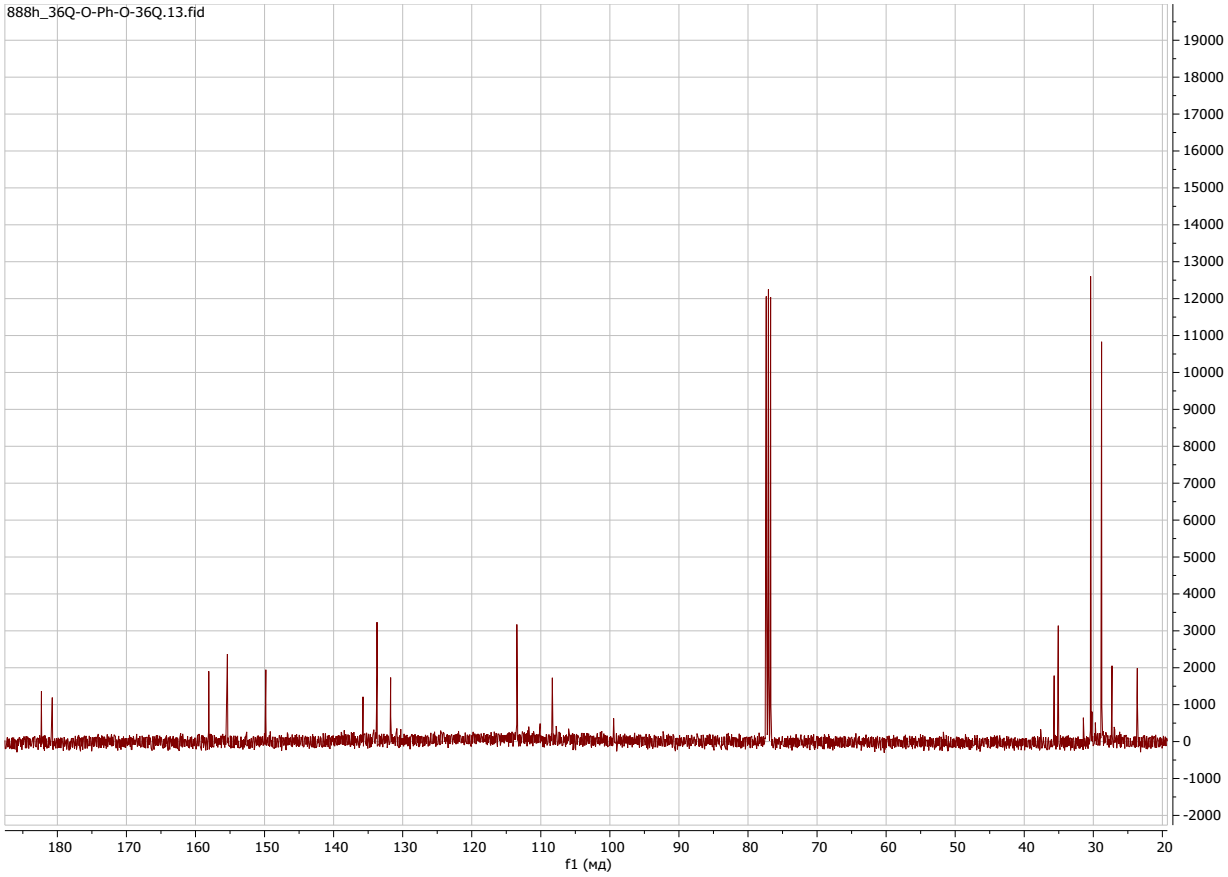

Figure. SI25. ^{13}C NMR spectrum of **1** ($CDCl_3$)

Magnetic measurements data.

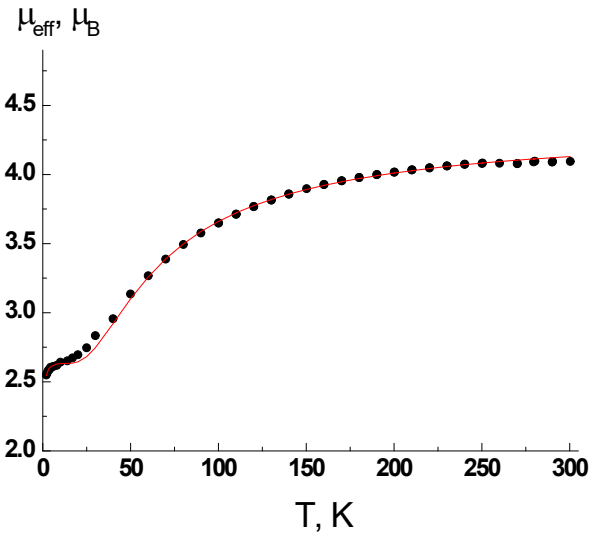

Figure. SI26. Thermal dependence of μ_{eff} for **2a** (circles), the red curve is an optimized fitting according H = $-2J_{Cu-SQ}\cdot(S_{SQ1}S_{Cu} + S_{Cu}S_{SQ2}) - 2J_{SQ-SQ}\cdot S_{SQ1}S_{SQ2})$ spin Hamiltonian and *g*-factor of Cu(II) ions and exchange interaction parameters J_{Cu-SQ}, J_{SQ-SQ} and zJ' are 2.167±0.006, –16.5±0.6 cm^{-1}, –32.8±0.9 cm^{-1} and –0.05±0.01 cm^{-1}.

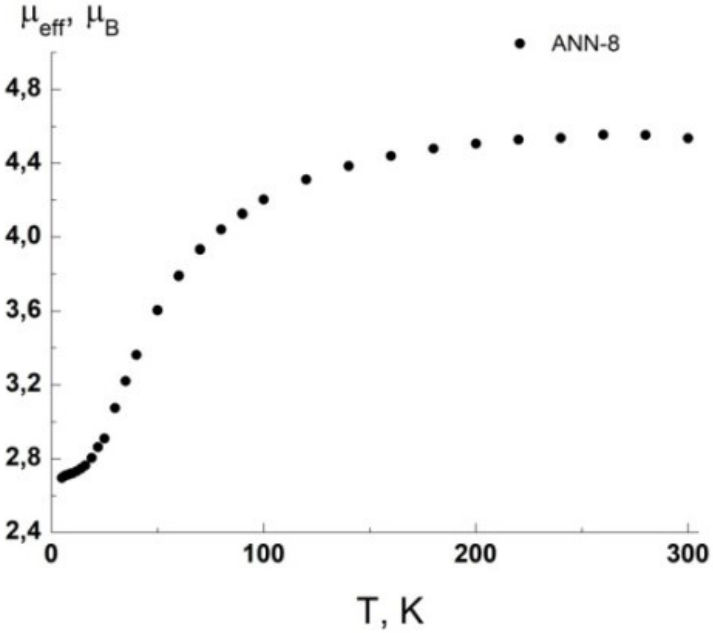

Figure. SI27. Thermal dependence of μ_{eff} for **2b**.

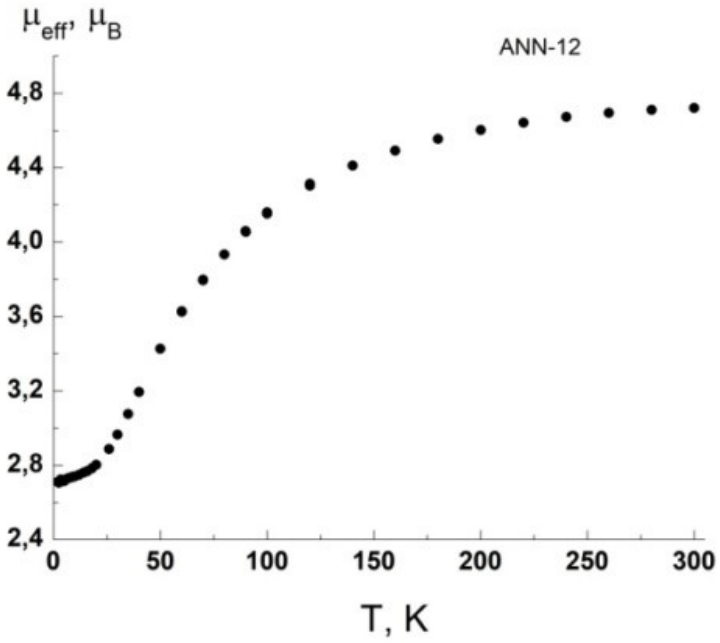

Figure. SI28. Thermal dependence of μ_{eff} for **2c**.

Electrospray Ionization Mass Spectrometry Analysis

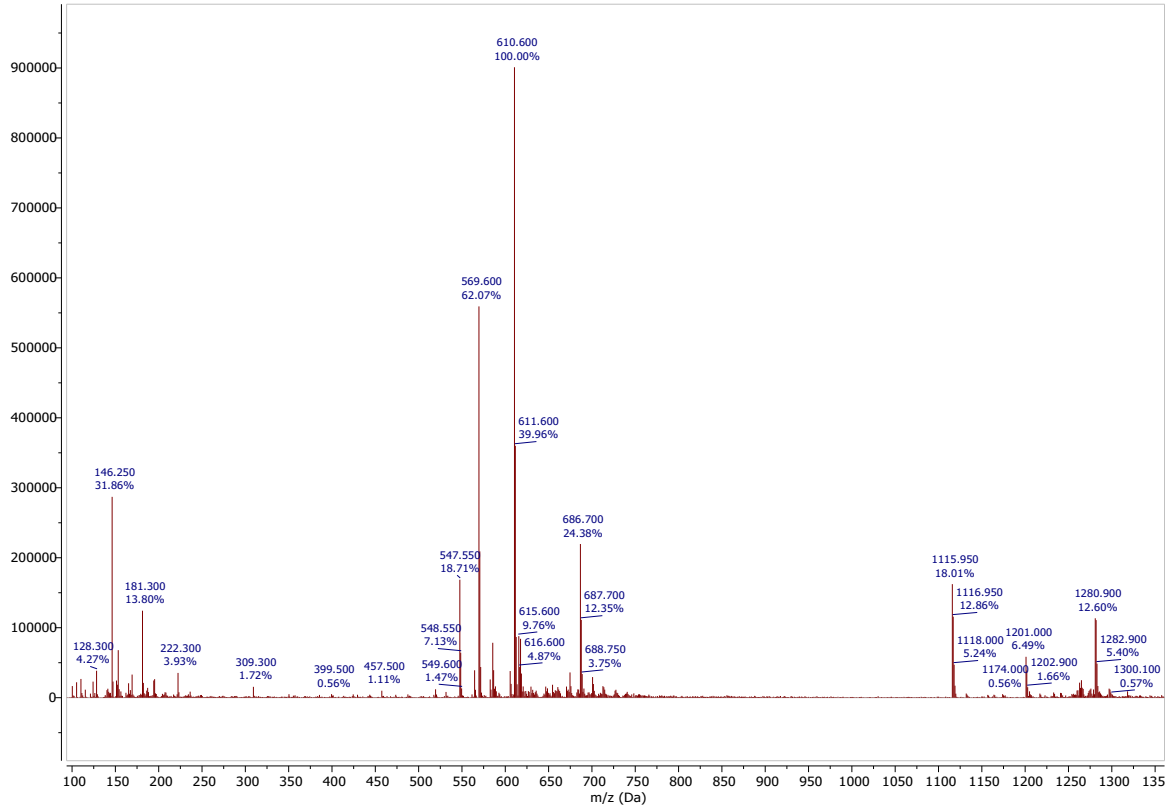

Figure. SI29. Positive-ion mode ESI-MS of **2a** in MeCN.

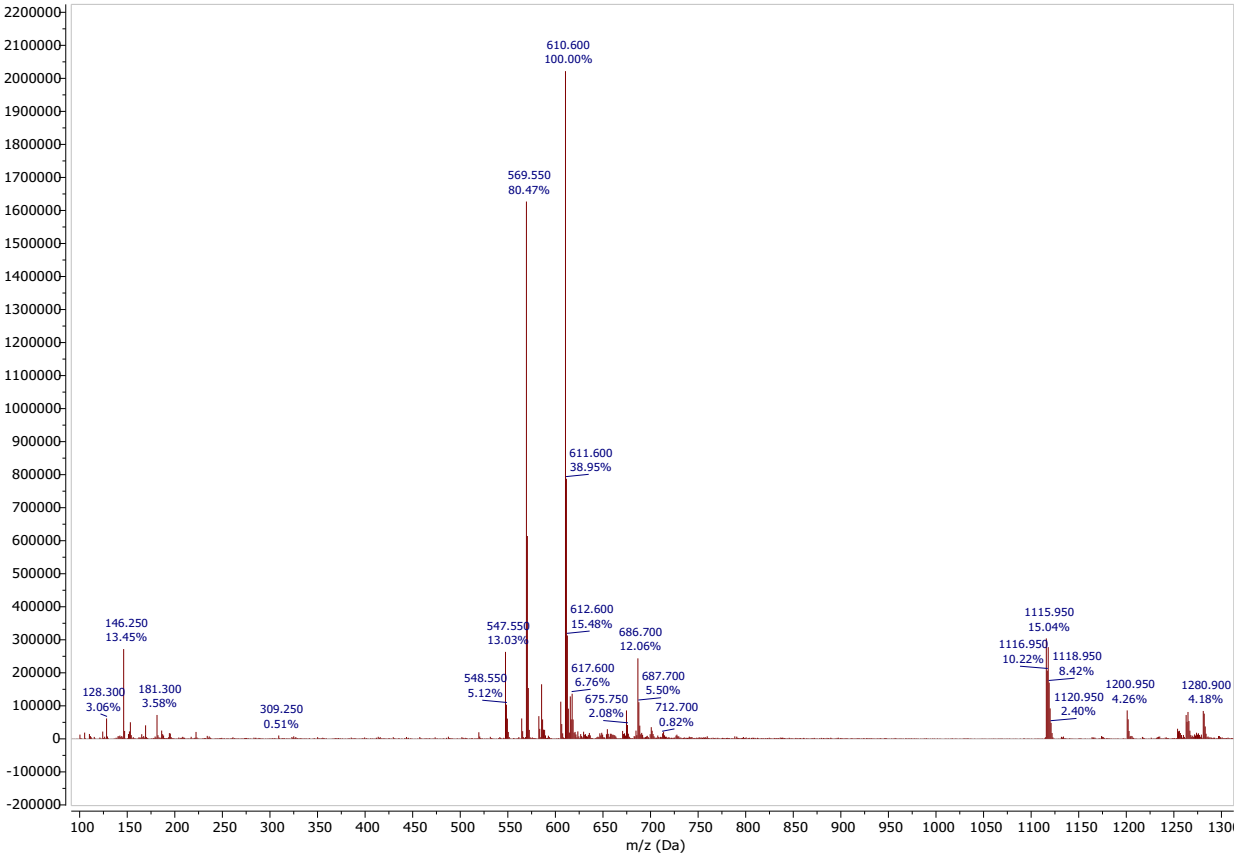

Figure. SI30. Positive-ion mode ESI-MS of **2a** in CH_2Cl_2.

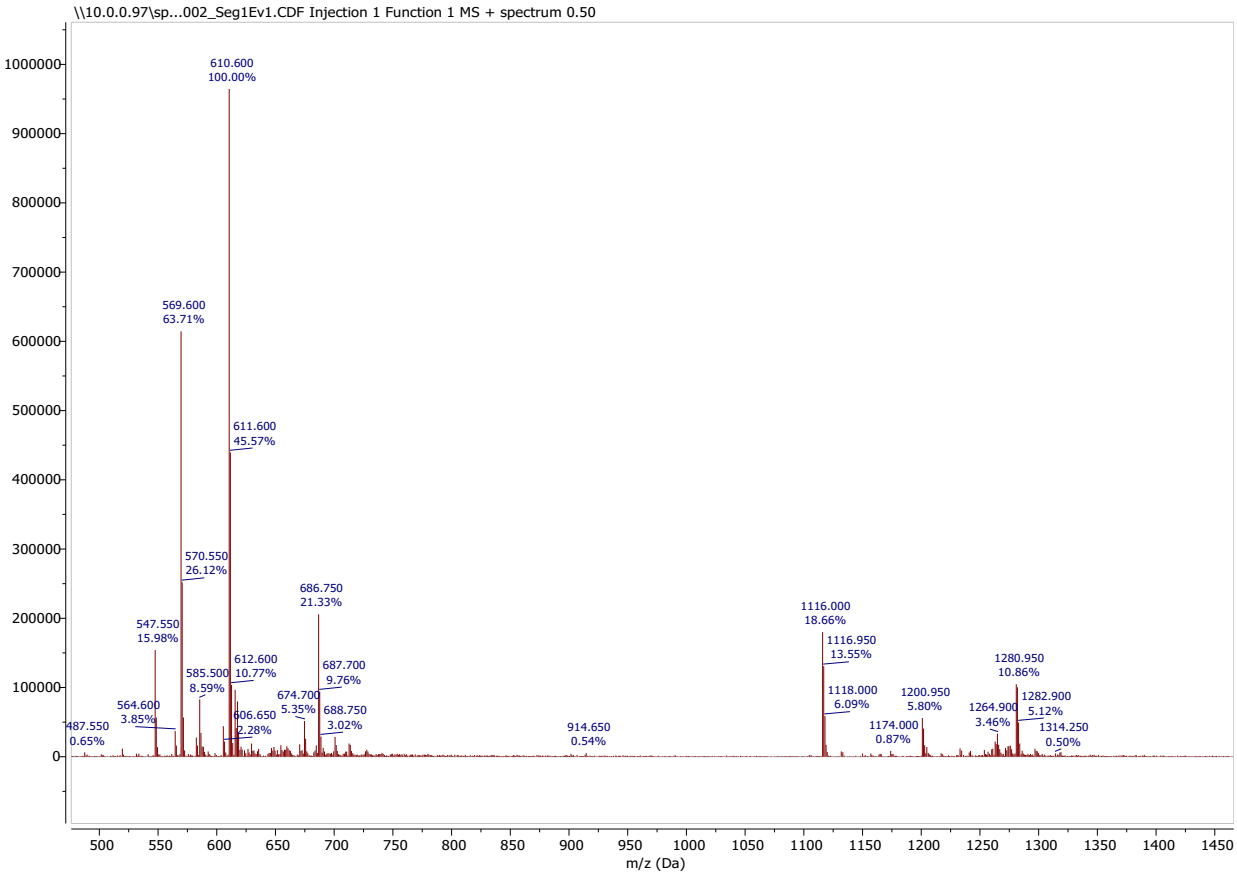

Figure. SI31. Positive-ion mode ESI-MS of **2b** in MeCN.

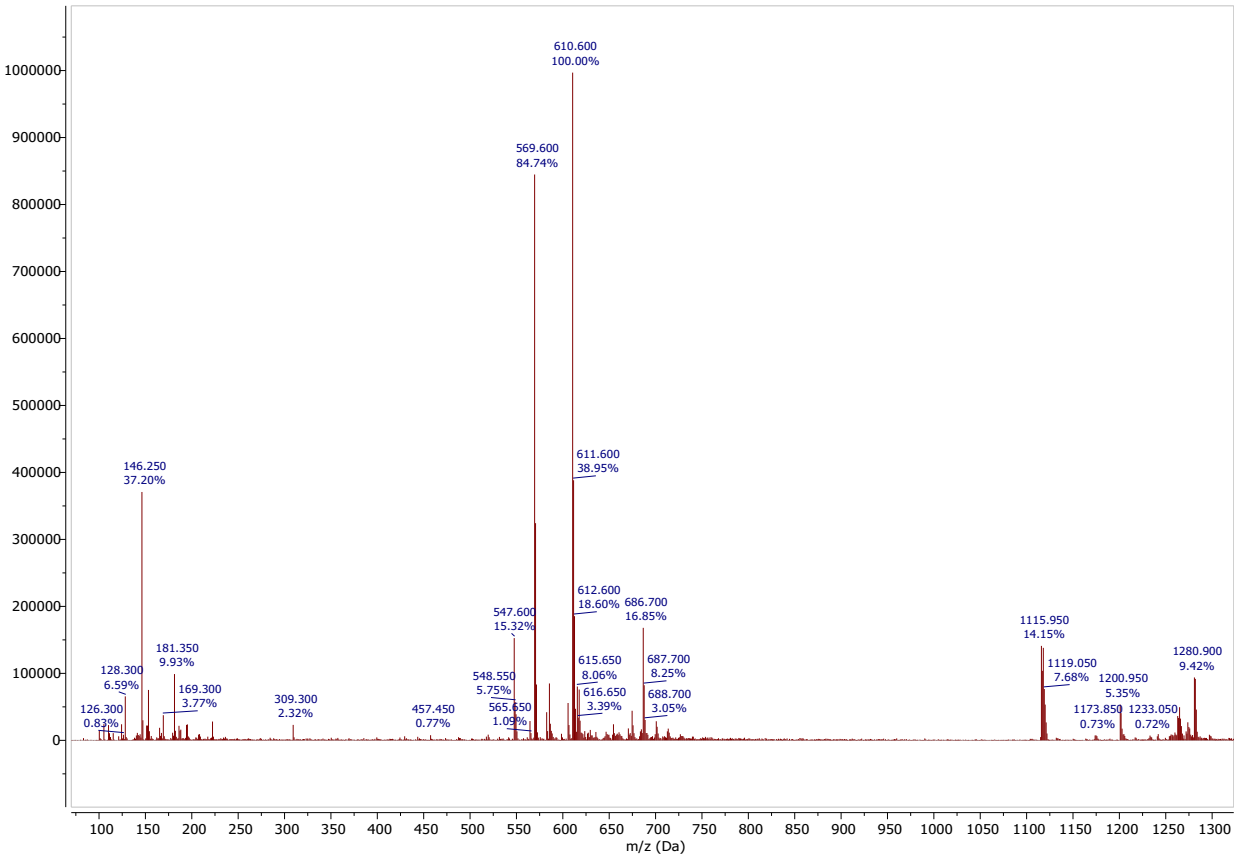

Figure. SI32. Positive-ion mode ESI-MS of **2b** in CH_2Cl_2.

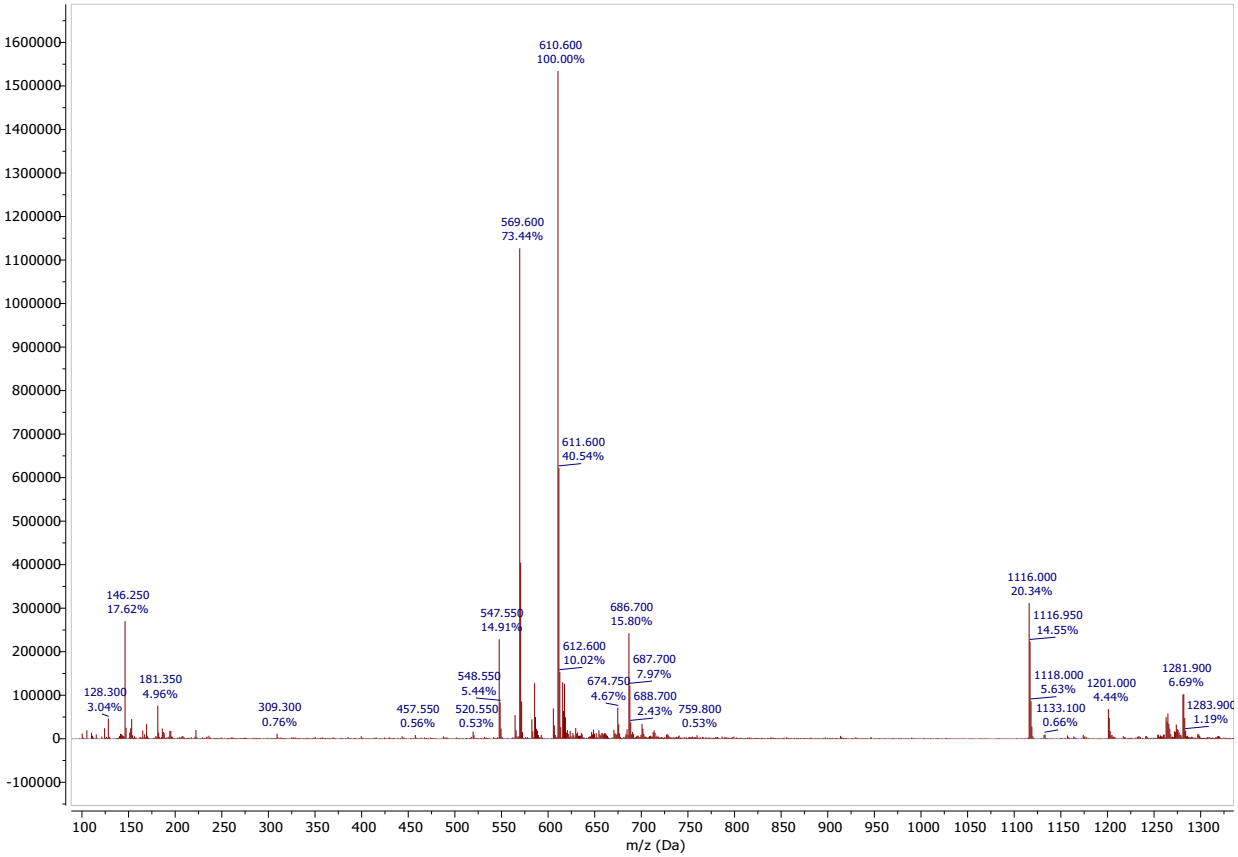

Figure. SI33. Positive-ion mode ESI-MS of **2c** in MeCN.

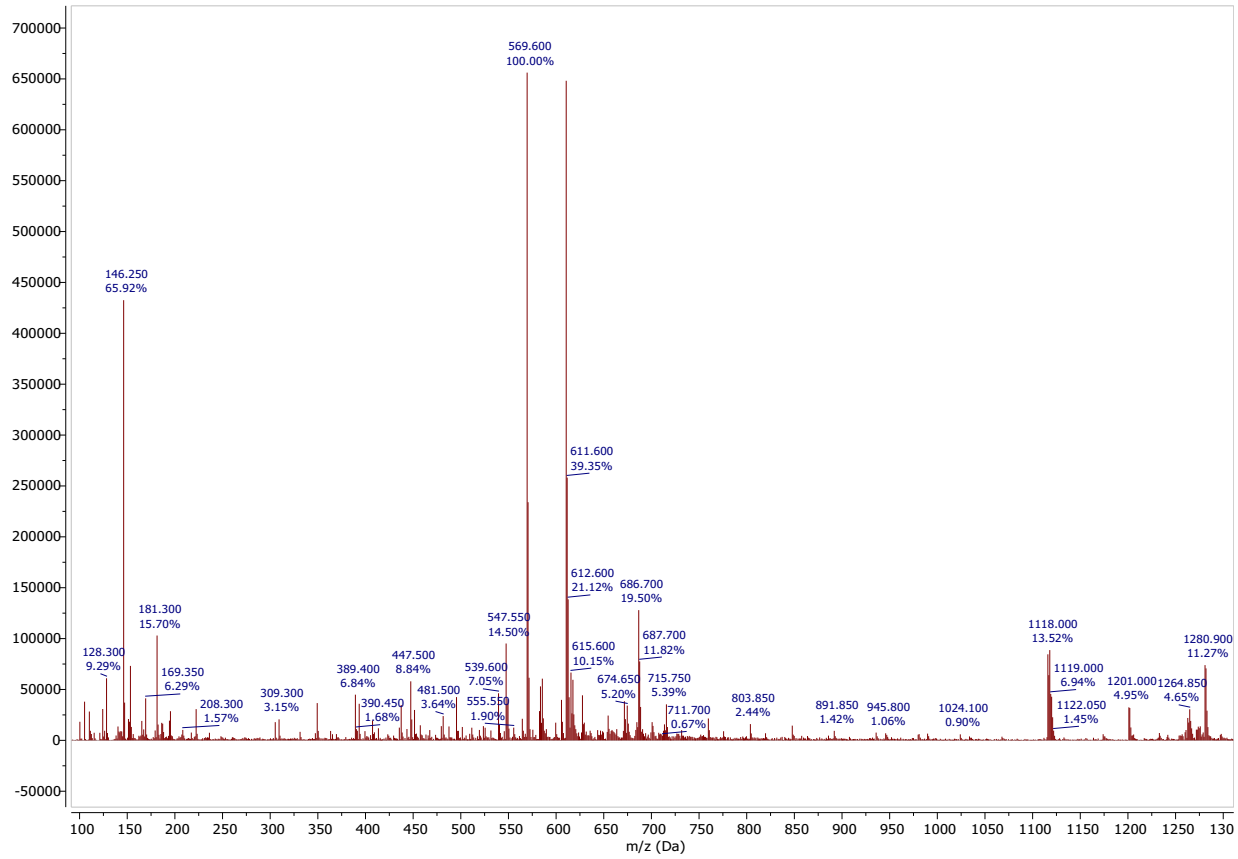

Figure. SI34. Positive-ion mode ESI-MS of **2c** in CH_2Cl_2.